Phase behavior of Lennard-Jones particles in two dimensions

Yan-Wei Li[1] and Massimo Pica Ciamarra[1,2,*]

[1]*Division of Physics and Applied Physics, School of Physical and Mathematical Sciences, Nanyang Technological University, Singapore 637371, Singapore*

[2]*CNR–SPIN, Dipartimento di Scienze Fisiche, Università di Napoli Federico II, I-80126, Napoli, Italy*

(Received 1 October 2020; accepted 4 November 2020; published 1 December 2020)

The phase diagram of the prototypical two-dimensional Lennard-Jones (LJ) system, while extensively investigated, is still debated. In particular, there are controversial results in the literature with regard to the existence of the hexatic phase and the melting scenario. Here we study the phase behavior of two-dimensional range-limited LJ particles via large-scale numerical simulations. We demonstrate that at a high temperature, when the attraction in the potential plays a minor role, melting occurs via a continuous solid-hexatic transition followed by a first-order hexatic-fluid transition. The hexatic phase occurs in a density range that vanishes as the temperature decreases so that at low-temperature melting occurs via a first-order liquid-solid transition. The temperature where the hexatic phase disappears is well above the liquid-gas critical temperature. The evolution of the density of topological defects confirms this scenario.

DOI: 10.1103/PhysRevE.102.062101

I. INTRODUCTION

The first experimental investigations of the melting transition of two-dimensional (2D) solids focused on rare gases adsorbed on graphite [1–3]. Since the Lennard-Jones (LJ) potential well describes the interaction potential between rare gases, these earlier studies triggered several numerical investigations of the phase diagram of two-dimensional LJ systems. These works followed through the years up to recent times [4–11]. Debates in the literature concerned the existence of the hexatic phase and the order of the transitions separating the hexatic and the liquid phase. One possibility is that, as suggested by the celebrated Kosterlitz-Thouless-Halperin-Nelson-Young (KTHNY) theory [12–14], melting occurs through a continuous solid-hexatic transition driven by the unbinding of dislocation pairs, followed by a continuous hexatic-liquid one driven by the further unbinding of isolated dislocation into disclinations. Alternatively, melting may follow the mixed or hard-disks [15–21] scenario, in which the solid-hexatic transition is continuous and the hexatic-liquid is discontinuous. Melting might also be discontinuous altogether, in which case there is no hexatic phase. These possible scenarios occur in inverse power-law repulsive systems, where the stiffness of the interaction potential fixes the melting path [16], and in hard polygons, where the melting scenario is controlled by the number of edges [18]. Besides, it is also possible that in LJ systems, and more generally in the presence of attractive forces, different melting scenarios occur in distinct regions of the phase diagram [22], given that both density and temperature changes induce melting.

The controversy concerning the features of the melting transition of 2D LJ solids is well illustrated by referring to two possible phase diagrams mentioned in the literature [23], which we reproduce in Fig. 1. In both phase diagrams, at very high temperature the hexatic is absent and the solid-liquid transition is discontinuous. Similarly, no hexatic phase occurs at low temperature, where one observes gas-solid coexistence. The hexatic phase is bounded by the gas-liquid coexistence curve in panel (a), or instead may interfere with the solid-liquid coexistence region as in panel (b). These are, we remark, just two of many possible [23,24] phase diagrams LJ systems might follow. Indeed, it is now well established that the hexatic region is not bounded at high temperature, as in this limit the attractive tail of the intermolecular potential is negligible, and LJ systems behave as a Weeks-Chandler-Anderson (WCA) system [25], whose interaction potential is obtained by truncating the LJ potential in its minimum, or equivalently, as a $1/r^{12}$ one. Recent works [16,26] have demonstrated that in these systems the hexatic phase is present. We note, however, that while these previous works reported a mixed order transition [16,26], at high temperature a recent investigation of the LJ phase diagram suggested the KTHNY one [11]. While the existence of the hexatic phase at high temperature is well established, this is not the case at low temperatures, when the attraction plays a role. Indeed, while some recent works support its existence [9,10], others do not [27,28].

II. MODEL AND METHODS

A. Simulation details

We study the phase behavior of 2D monodisperse particles of mass m, interacting with a truncated LJ potential:

$$U(r) = \begin{cases} 4\epsilon[(\sigma/r)^{12} - (\sigma/r)^6 + C] & r \leqslant r_c \\ 0 & \text{otherwise,} \end{cases} \quad (1)$$

*massimo@ntu.edu.sg

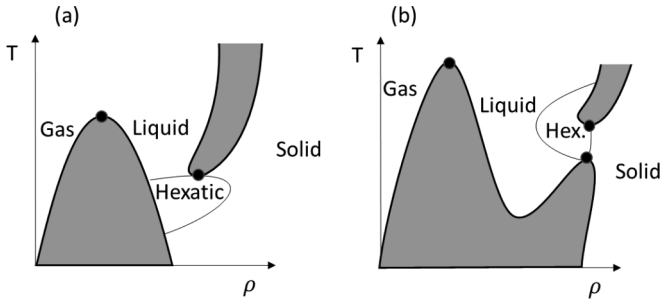

FIG. 1. Speculated phase diagrams of the two-dimensional LJ systems in a T-ρ plane [23]. The shadowed regions indicate phase coexistence.

where $r_c = 2.5\sigma$, and C is a constant chosen such that $U(r_c) = 0$. While we do not consider the influence of the adopted truncation scheme, previous results indicate that changes in r_c may quantitatively influence the phase diagram [29]. σ, m, and $\sqrt{m\sigma^2/\epsilon}$ will be our units of length, mass, and time, respectively. We mainly consider a system with $N = 318^2$ particles in a rectangular box with side length ratio $L_x : L_y = 2 : \sqrt{3}$. Different system sizes ranging from $N = 32^2$ to $N = 512^2$ are additionally studied to investigate finite-size effects.

We equilibrate and sample the system in the canonical ensemble via molecular dynamics simulations. The equations of motion are integrated via a Verlet algorithm [30], and the temperature is fixed via the Nosé-Hoover thermostat [30]. We perform the simulations with the GPU-accelerated GALAMOST package [31].

B. Identification of the different phases

The spatial decay of the translational and bond-orientational correlation functions allows distinguishing the solid, hexatic, and liquid phases. The translational correlation function is $c(r) = \langle e^{i\vec{G}\cdot(\vec{r}_k - \vec{r}_l)}\delta(r - |\vec{r}_k - \vec{r}_l|)\rangle$, where $\vec{G}$ is one of the first Bragg peaks, identified by the static structure factor [15,32]. The bond-orientational correlation function is $g_6(r = |\vec{r}_i - \vec{r}_j|) = \langle \psi_6(\vec{r}_i)\psi_6^*(\vec{r}_j)\rangle$, where $\psi_6(\vec{r}_i)$ is the bond-orientational order parameter of particle i, defined as $\psi_6(\vec{r}_i) = \frac{1}{n}\sum_{m=1}^{n} \exp(i6\theta_m^i)$. Here n is the number of nearest neighbors of the particle and θ_m^i is the angle between $(\vec{r}_m - \vec{r}_i)$ and a fixed arbitrary axis.

In the solid phase, Mermin-Wagner theorem [33] prevents the existence of long-range translational order, and $c(r) \propto r^{-\eta}$ with $\eta \leqslant 1/3$, indicating quasi-long-range translational order. Conversely, $g_6(r)$ does not decay as the bond-orientational order is long ranged. In the hexatic phase there is an exponential decay in $c(r)$, i.e., $c(r) \propto \exp(-r/\xi)$, and a power-law decay in $g_6(r)$, $g_6(r) \propto r^{-\eta_6}$ with $0 < \eta_6 \leqslant 1/4$, representing a short-range translational order and a quasi-long-range bond-orientational order. In the liquid phase, both the translational and the bond-orientational orders are short ranged, and both $c(r)$ and $g_6(r)$ decay exponentially.

We identify the coexistence region investigating the equation of state, which needs to exhibit a Mayer-Wood loop. The Mayer-Wood loop results from the interfacial free energy between coexistence phases and thus is a signature of the first-order transition. The coexistence phase is within this loop, with the phase boundary determined via the Maxwell construction. Furthermore, we study the probability distribution of the local density, which is bimodal in the coexistence region. The local density for each particle is defined as $\rho(\vec{r}_i) = \frac{\sum_{j=1}^{N} H(r_l - |\vec{r}_i - \vec{r}_j|)}{\pi r_l^2}$, where H is the Heaviside step function, $r_l = 50$ for the system with $N = 318^2$ and 5 for the system with $N = 32^2$. The choice of r_l does not affect these results unless r_l becomes tiny or of the order of the system size.

III. RESULTS

A. Gas-liquid transition

We begin by briefly reviewing our results for the gas-liquid transition. We illustrate in Fig. 2(a) the pressure dependence on the density and demonstrate in Figs. 2(b) and 2(c) the probability distribution of the local density and of the local bond-orientational order parameter, at $\rho \simeq 0.25$, and at temperatures $T = 0.5$, $T = 0.45$, and $T = 0.42$, for a system of $N = 1024$ particles. Snapshots of the systems are in Fig. 2(d). The coexistence region is clearly revealed by the almost density independence of the pressure, the concomitant bimodal density distribution, and the emergence of a heterogeneous distribution of particles in the snapshot. We determine the phase boundaries via the Maxwell construction and use a polynomial fit of these points to approximate the coexistence curve close to the critical point, which we estimate to occur at ($\rho_c \simeq 0.366$, $P_c \simeq 0.042$). Previous studies found comparable results [4,5,7,8,34].

In the $N = 1024$ system, at low temperature $T = 0.42$, the pressure is negative at large enough density, as apparent in Fig. 2(a). This is a finite-size effect, as pressure stays positive as thermodynamics dictates, for $N = 128^2$ [black triangles at $T = 0.42$ in Fig. 2(a)]. This system-size-dependent behavior is not expected in the liquid or gas-liquid coexistence region, as these phases have small correlation lengths. Instead, this result indicates that $T = 0.42$ is below the triple point and that the coexisting phases are of gas and solid type. This claim is supported by the probability distribution of the local bond-orientational order parameter $p(q_6)$, where we observe at $T = 0.42$ a pronounced peak at $q_6 > 0.7$ corresponding to well-ordered particles. This well-ordered region is absent at higher temperatures, e.g., at $T = 0.50$ and $T = 0.45$. The temperature of the triple point is therefore in the range $T = [0.42 : 0.45]$.

B. Temperature dependence of the two-dimensional melting

1. Phase determination

We investigate the melting transition of 2D LJ solids, first focusing on a high-temperature value, $T = 10.0$, where attractive forces are negligible. At this value of the temperature, we observe a clear Mayer-Wood loop in the equation of state, indicating phase coexistence, as in Fig 3(a). We use Maxwell's construction to locate the phase boundaries, having approximated the equation of state via a fifth-order polynomial. The spatial decay of the translational and bond-orientational correlation functions then allows identifying the coexisting pure phases. The behavior of these quantities is illustrated

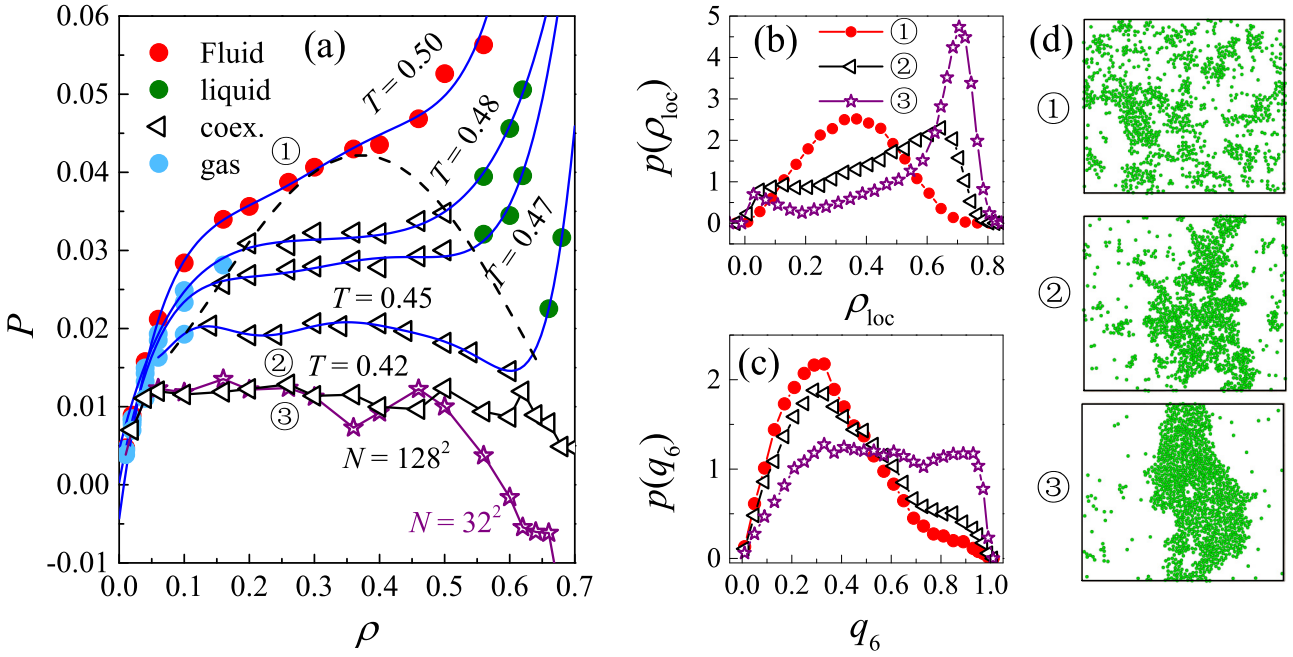

FIG. 2. Condensation transition. Panel (a) illustrates the equation of state at different temperatures. Different symbols correspond to different phases, as in the legend. Blue lines are polynomial fits to the equation of state, while the black and the purple lines connecting at $T = 0.42$ are guides to the eye. The black dashed line is a polynomial fit of the coexistence boundary, according to which the critical point is at ($\rho_c \simeq 0.366$, $P_c \simeq 0.042$). Panels (b) and (c) illustrate the probability distribution of the local density and that of the local bond-orientational order parameter at $\rho \simeq 0.25$ and $T = 0.5$①, $T = 0.45$②, and $T = 0.42$③ . Panel (d) illustrates snapshots of the system.

in Figs. 3(b) and 3(c). Both correlation functions decay exponentially in the low-density coexisting phase, which is therefore of liquid type. In the high-density coexisting phase $c(r)$ decays exponentially while $g_6(r)$ decays as a power law with the exponent $\eta_6 < 1/4$. Accordingly, the coexisting phases are of fluid and hexatic type. The system-size scaling

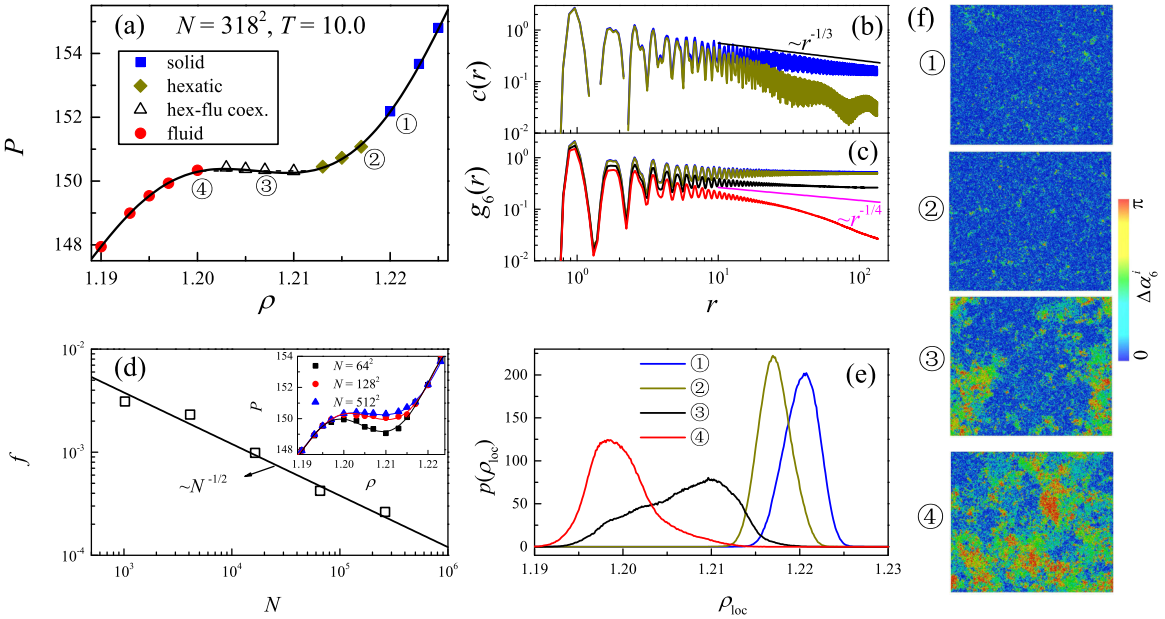

FIG. 3. Melting transition at $T = 10.0$. Panel (a) illustrates the equation of state for a system with $N = 318^2$ particles. Different symbols indicate the different phases, as shown in the legend. The black line is a fifth-order polynomial fit. Panels (b) and (c) illustrate the translational correlation function $c(r)$ and the bond-orientational one $g_6(r)$ at different densities, as indicated in (a). Panel (d) illustrates the system-size dependence of the interfacial free energy f and of the equation of state (inset). Panel (e) shows the distribution of the local density at selected state points, as indicated in (a). Panel (f) illustrates snapshots of the system with particles color coded according to the angle $\Delta\alpha_4^i$ between their local bond-orientational order parameter, and the global one.

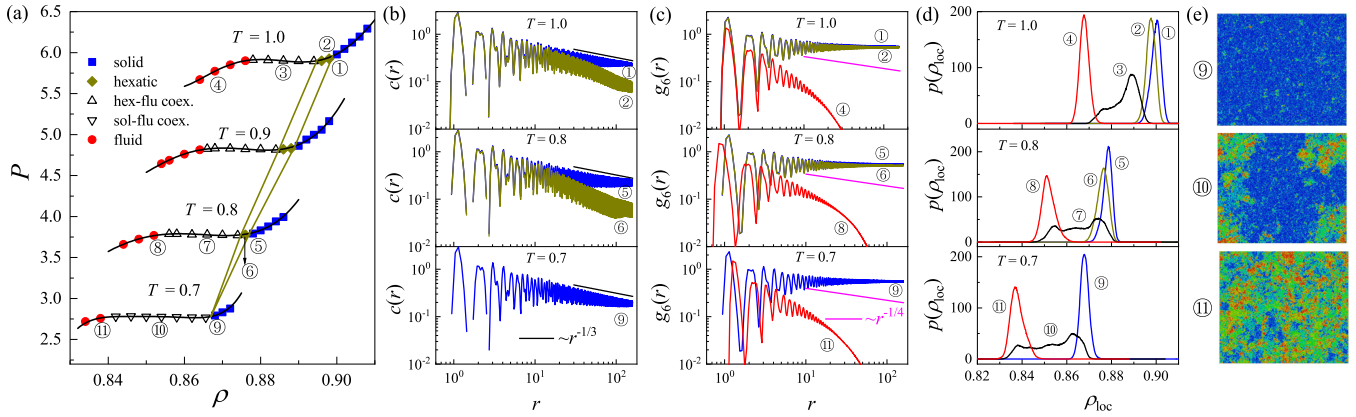

FIG. 4. Temperature dependence of the melting transition. Panel (a) illustrates the equation of state at several temperatures, with different symbols corresponding to different phases, as in the legend. Black lines are polynomial fits. Panels (b) and (c) illustrate the translational and the bond-orientational correlation functions at selected state points, as indicated in (a). Panel (d) shows the probability distribution of the local density, and panel (e) a snapshot of the system colored as in Fig. 3(f).

of the interfacial free energy f determined from the area covered by the up bump of the Mayer-Wood loop and the horizontal line from the Maxwell construction further support the first-order nature of the hexatic-fluid transition. We find $f \propto N^{-1/2}$, as illustrated in Fig. 3(c), providing robust evidence for a discontinuous hexatic-fluid transition at $T = 10.0$ [15,34]. Consistently with this result, the probability distribution of the local density $p(\rho_{\rm loc})$ has a unimodal Gaussian-like shape in the pure phases; conversely, it is broad, almost bimodal, in the coexistence region. As the density increases further, the system continuously transitions into the solid phase. Here $c(r)$ decays algebraically with the exponent $\eta \leqslant 1/3$, while $g_6(r)$ does not decay.

We illustrate the different states by color-coding each particle according to the angle $\Delta\alpha_6^i$ between the global $\vec{\Psi}_6 = \frac{1}{N}\sum_i \psi_6(\vec{r}_i)$ and the local $\psi_6(\vec{r}_i)$ bond-orientational parameters, $\psi_6(\vec{r}_i)\cdot\vec{\Psi}_6^* = |\psi_6(\vec{r}_i)||\vec{\Psi}_6^*|\cos(\Delta\alpha_k^i)$. We observe a uniform blue color in the solid and hexatic [Fig. 3(f), ① and ②], reflecting the long range or quasi long range of the bond-orientational order. In the fluid phase, Fig. 3(e) ④, the snapshot appears almost randomly colored due to the short range of the bond-orientational order. In the coexistence of the hexatic and fluid phases, Fig. 3(e) ③, patches with a uniform color and randomly colored regions coexist.

These results demonstrate that at high temperature where attractive forces play a minor role, LJ solids melt via a mixed melting scenario. This finding agrees with previous investigations of the $1/r^{12}$ [16] and WCA [26] systems but contrasts with [11], which claimed the hexatic-fluid transition to be continuous. Reference [11] found different results as it assumed $\vec{G}$, which enters the definition of the translational correlation function, to be parallel to the global bond-orientational order parameter $\vec{\Psi}_6$. This approximation holds for hard-disk [16] but not for LJ particles. See Ref. [32] for details.

The high-temperature melting scenario gets modified as the temperature decreases, as we illustrate in Fig. 4, where we report the equation of state (a) for different temperatures, the translational (b) and bond-orientational (c) correlation functions, the local density probability distribution (d), and snapshots of the system with particles color-coded as in Fig. 3. Melting involves a discontinuous transition at all temperatures, as apparent from the equation of state (a) and the distribution of the local density (d); the low-density coexisting phase is, of course, always of liquid type. The analysis of the correlation functions indicates that the high-density coexisting phase is hexatic for $T \simeq 0.7$ and solid at lower temperatures. Indeed, only at higher temperatures (e.g., ② and ⑥) does the high-density coexisting phase have an exponentially decaying $c(r)$ and an algebraically (or extended) decaying $g_6(r)$. The width of the density range where the hexatic phase occurs therefore shrinks as the temperature decreases, until it disappears at $T \simeq 0.7$.

The direct visualization of the system with particles color-coded according to $\Delta\alpha_6^i$ supports the above identification of the phases. We observe a uniform blue color in the solid phase (⑨), uncorrelated colors in the fluid phase (⑪), and uncorrelated patches on a blue background in the fluid-solid coexistence region (⑩).

2. *Topological defects*

The evolution of the density of topological defects across the melting transition further allows distinguishing the different melting scenarios. Topological defects are particles whose number of nearest neighbors, which we determine via the Voronoi construction, differs from six. While fluids might have isolated defects, disclinations in the hexatic phase defects must mainly appear in dislocations ($5-7$ pairs) and in dislocation pairs ($5-7-5-7$ quartets), which do affect the translational order. In the solid, ideally, no defects are expected. We investigate the fraction of isolated dislocations and isolated disclinations during density-driven melting transitions at a high temperature, where the melting is of hard-disk type, and at a low temperature, where melting occurs through a first-order solid-liquid transition with no hexatic phase.

At high temperature, $T = 1.0$, isolated dislocations start growing on decreasing the density at $\rho = 0.90$, which corresponds to the solid-hexatic transition density. Conversely, the fraction of disclinations starts growing when the system enters

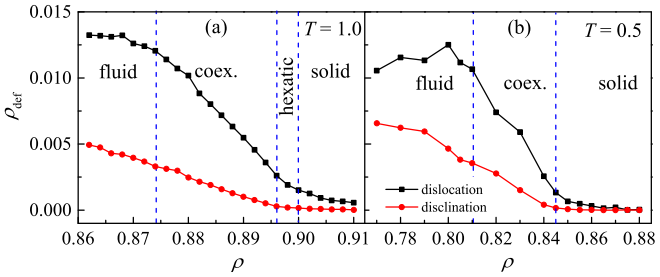

FIG. 5. Probability distribution of the cluster size of defective particles $p(N_c)$ for selected densities in different phases at (a) $T = 1.0$ and (b) $T = 0.5$. $p(N_c)$ shows an exponential decay as indicated by the solid lines in both (a) and (b). Panels (c) and (d) illustrate the density dependence of the mean cluster size $\langle N_c \rangle$, at $T = 1.0$ and $T = 0.5$.

the hexatic-fluid coexistence region at $\rho = 0.896$. This result is in line with the expected presence [12–14] of a finite fraction of isolated dislocation and very few isolated disclinations in the hexatic phase. In the coexistence phase, the relative amount of fluidlike and hexaticlike particles varies linearly with the density. Consistently, the density of dislocations and that of disclinations varies approximately linearly with the density. At low temperature, $T = 0.5$, the fraction of dislocations and that of disclinations start growing at the low-density limit of the solid phase, again supporting the absence of the hexatic phase.

Besides occurring isolated and in small clusters, defective particles can also agglomerate in large ones. Large clusters are not accounted for in the original KTHNY theory [12–14], but have been observed in systems with power-law interactions [16,35], in hard regular polygons [18], and recently in both passive and active stiff particles [35]. Here we consider the evolution of the cluster size probability distribution $p(N_c)$

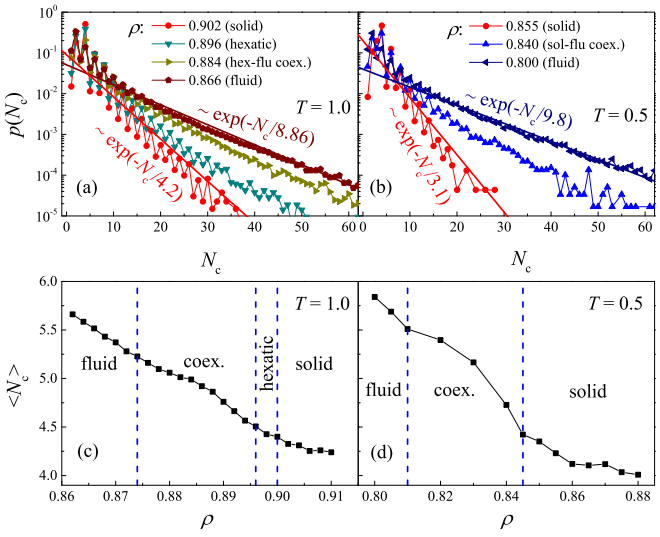

FIG. 6. The density dependence of the fraction of isolated dislocations (black squares) and isolated disclinations (red circles) at (a) $T = 1.0$ and (b) $T = 0.5$. The blue dashed lines separate different phases.

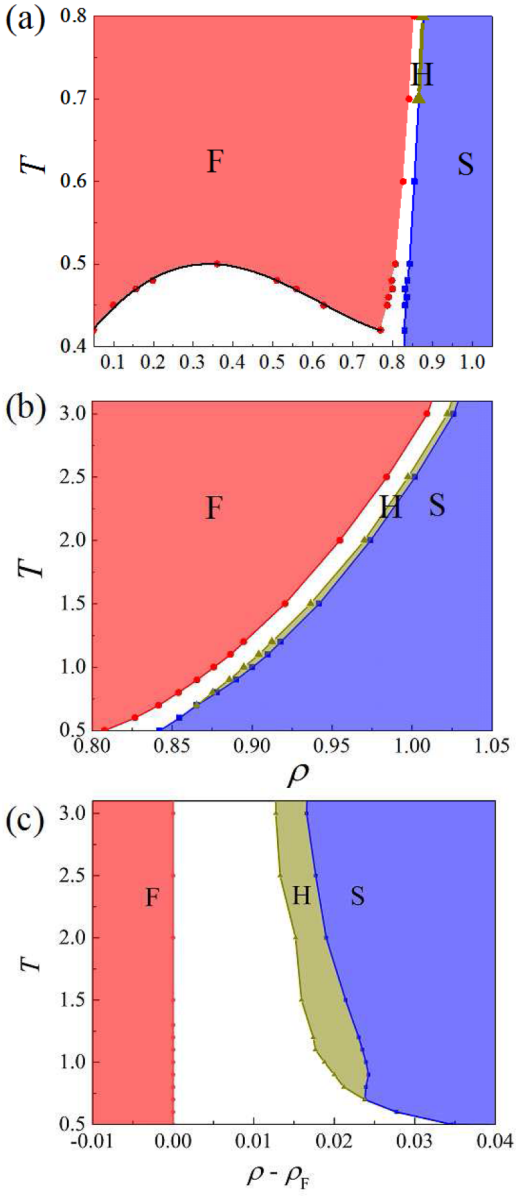

FIG. 7. Phase diagram two-dimensional LJ particles. Panel (a) focuses on the whole $T - \rho$ plane, while panel (b) is a zoom on the high-temperature high-density region where the hexatic phase emerges. In panel (c) the phase diagram is plotted in the T vs $\rho - \rho_F$ plane, where ρ_F is the coexistence density of the fluid phase. At each investigated temperature, we mark with symbols the estimated phase boundaries. We use colors to distinguish the pure phases, fluid (F), solid (S), and hexatic (H). Coexistence regions, including hexatic-fluid, solid-fluid, and liquid-gas coexistence, are white.

during the high- and the low-temperature melting transitions considered in Fig. 5.

The cluster size probability distribution decays exponentially, regardless of the phase of the system, both at high and at small temperature, as we illustrate in Figs. 6(a) and 5(b), respectively. This finding contrasts with the recent observations, in both systems of stiff and soft repulsive particles, of a power-law cluster size distribution close to the hexatic-liquid phase boundary [35]. In this work, however, clusters

are defined via a coarse-grained procedure so that defective particles may be assigned to a same cluster even if not nearest neighbors. This suggests that the observed difference stems from the different operative definition of clusters of defects.

The exponential decay of the cluster size distribution is controlled by the size of the average cluster $\langle N_c \rangle$, which increases as the system melts, as we illustrate in Fig. 6(c) for $T = 1.0$ and in Fig. 6(d) for $T = 0.5$. In the high-density solid phases $\langle N_c \rangle \simeq 4$, as expected considering that bounded dislocation pairs, which involve four defected particles, dominate in the solid phase. As the density decreases, $\langle N_c \rangle$ grows significantly in the fluid and coexistence phases. These observations do not depend on the existence of the hexatic phase and the melting scenario.

IV. CONCLUSIONS

We summarize our findings on the phase behavior of 2D LJ particles in the phase diagram presented in Fig. 7, which markedly differs from previously speculated one shown in Fig. 1. Panel (a) illustrates the phase diagram in the temperature range between 0.4 and 0.8 to highlight the liquid-gas coexistence region. Panel (b) focuses on the high-temperature and high-density region, where the hexatic phase appears. Panel (c), which focuses on the same region, illustrates the phase diagram in the T and $\rho - \rho_F$ plane, where ρ_F is the high-density limit of the fluid phase, to highlight the hexatic region. The phase diagram reveals two important features.

First of all, at high temperature, when the attraction in the LJ potential plays a minor role, the system melt occurs via a mixed scenario with a continuous solid-hexatic transition and a first-order hexatic-fluid transition. This melting scenario occurs in the $1/r^{12}$ and WCA systems [16,26]. In this limit, the density range where the hexatic phase occurs has a constant width.

Second, as the temperature decreases the solid-hexatic and the hexatic-fluid transition densities decrease at different rates so that the hexatic density range shrinks. The hexatic phase disappears at $T = 0.7$, below which melting occurs via a first-order solid-fluid transition. We remark that the temperature where the hexatic phase vanishes is much higher than the critical temperature, $T \simeq 0.496$.

The proliferation of topological defects drives the melting transition. In agreement with the KTHNY theory, we observed in the hexatic phase isolated dislocations and virtually no isolated disclinations. In the coexistence regions, both kinds of defects are present, and their density varies linearly with the density. While clusters involving more than a few defective particles are always present, we have found the cluster size distribution to be always exponential, with a characteristic size continuously growing as the system melt. Hence in this system melting does not result from a percolation transition of defective particles.

ACKNOWLEDGMENTS

We acknowledge support from the Singapore Ministry of Education through the Academic Research Fund (Tier 2) MOE2017-T2-1-066 (S), and are grateful to the National Supercomputing Centre (NSCC) of Singapore for providing computational resources.

[1] W. F. Brinkman, D. S. Fisher, and D. E. Moncton, Science **217**, 693 (1982).
[2] P. A. Heiney, P. W. Stephens, R. J. Birgeneau, P. M. Horn, and D. E. Moncton, Phys. Rev. B **28**, 6416 (1983).
[3] K. J. Strandburg, Rev. Mod. Phys. **60**, 161 (1988).
[4] J. A. Barker, D. Henderson, and F. F. Abraham, Physica A **106**, 226 (1981).
[5] B. Smit and D. Frenkel, J. Chem. Phys. **94**, 5663 (1991).
[6] R. R. Singh, K. S. Pitzer, J. J. d. Pablo, and J. M. Prausnitz, J. Chem. Phys. **92**, 5463 (1990).
[7] X. Feng, Z. Li, and Z. Guo, Chin. Sci. Bull. **45**, 2004 (2000).
[8] J. M. Phillips, L. W. Bruch, and R. D. Murphy, J. Chem. Phys. **75**, 5097 (1981).
[9] H. Shiba, A. Onuki, and T. Araki, Europhys. Lett. **86**, 66004 (2009).
[10] K. Wierschem and E. Manousakis, Phys. Rev. B **83**, 214108 (2011).
[11] A. Hajibabaei and K. S. Kim, Phys. Rev. E **99**, 022145 (2019).
[12] J. M. Kosterlitz and D. J. Thouless, J. Phys. C **6**, 1181 (1973).
[13] B. I. Halperin and D. R. Nelson, Phys. Rev. Lett. **41**, 121 (1978).
[14] A. P. Young, Phys. Rev. B **19**, 1855 (1979).
[15] E. P. Bernard and W. Krauth, Phys. Rev. Lett. **107**, 155704 (2011).
[16] S. C. Kapfer and W. Krauth, Phys. Rev. Lett. **114**, 035702 (2015).
[17] Y.-W. Li and M. P. Ciamarra, Phys. Rev. Materials **2**, 045602 (2018).
[18] J. A. Anderson, J. Antonaglia, J. A. Millan, M. Engel, and S. C. Glotzer, Phys. Rev. X **7**, 021001 (2017).
[19] M. Zu, J. Liu, H. Tong, and N. Xu, Phys. Rev. Lett. **117**, 085702 (2016).
[20] J. Russo and N. B. Wilding, Phys. Rev. Lett. **119**, 115702 (2017).
[21] A. L. Thorneywork, J. L. Abbott, D. G. A. L. Aarts, and R. P. A. Dullens, Phys. Rev. Lett. **118**, 158001 (2017).
[22] Y.-W. Li and M. P. Ciamarra, Phys. Rev. Lett. **124**, 218002 (2020).
[23] D. R. Nelson, *Defects and Geometry in Condensed Matter Physics* (Cambridge University Press, Cambridge, England, 2002).
[24] D. R. Nelson and B. I. Halperin, Phys. Rev. B **19**, 2457 (1979).
[25] J. D. Weeks, D. Chandler, and H. C. Andersen, J. Chem. Phys. **54**, 5237 (1971).
[26] S. S. Khali, D. Chakraborty, and D. Chaudhuri, arXiv:2007.00297.
[27] D. Du, M. Doxastakis, E. Hilou, and S. L. Biswal, Soft Matter **13**, 1548 (2017).

[28] B. Li, X. Xiao, S. Wang, W. Wen, and Z. Wang, Phys. Rev. X **9**, 031032 (2019).
[29] B. Smit, J. Chem. Phys. **96**, 8639 (1992).
[30] M. Allen, *Computer Simulation of Liquids* (Oxford University Press, Oxford, England, 1987).
[31] Y. Zhu, H. Liu, Z. Li, H. Qian, G. Milano, and Z. Lu, J. Comput. Chem. **34**, 2197 (2013).
[32] Y.-W. Li and M. P. Ciamarra, Phys. Rev. E **100**, 062606 (2019).
[33] N. D. Mermin and H. Wagner, Phys. Rev. Lett. **17**, 1133 (1966).
[34] M. Schrader, P. Virnau, and K. Binder, Phys. Rev. E **79**, 061104 (2009).
[35] P. Digregorio, D. Levis, L. F. Cugliandolo, G. Gonnella, and I. Pagonabarraga, arXiv:1911.06366.